Energy & Environmental Science

www.rsc.org/ees

Volume 6 | Number 6 | June 2013 | Pages 1643–1972

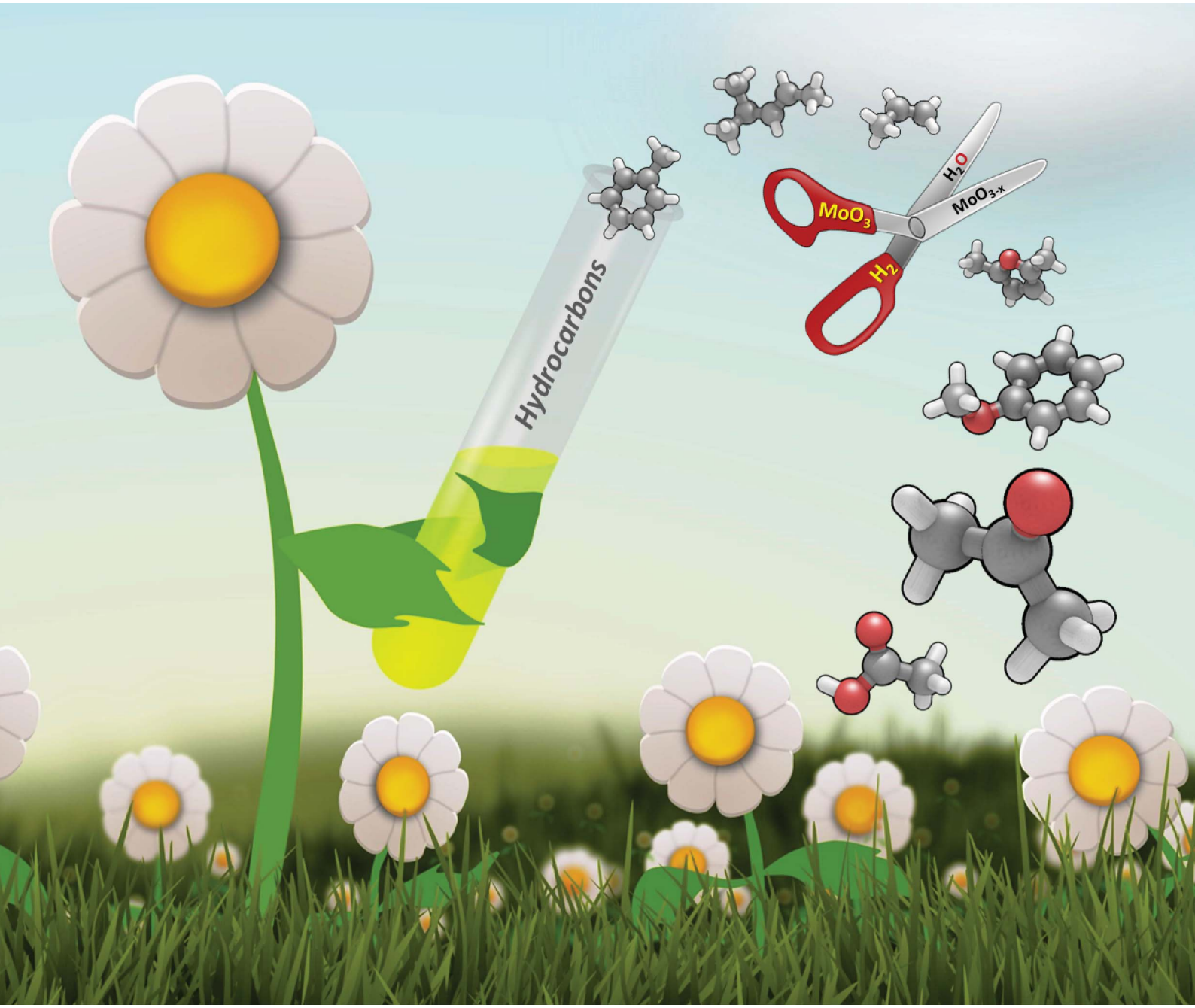

ISSN 1754-5692

RSC Publishing

COMMUNICATION

Román-Leshkov *et al.*

Effective hydrodeoxygenation of biomass-derived oxygenates into unsaturated hydrocarbons by MoO_3 using low H_2 pressures

Energy & Environmental Science

RSC Publishing

COMMUNICATION

View Article Online
View Journal | View Issue

Effective hydrodeoxygenation of biomass-derived oxygenates into unsaturated hydrocarbons by MoO_3 using low H_2 pressures†

Cite this: *Energy Environ. Sci.*, 2013, **6**, 1732

Received 14th December 2012
Accepted 8th April 2013

DOI: 10.1039/c3ee24360e

www.rsc.org/ees

Teerawit Prasomsri, Tarit Nimmanwudipong and Yuriy Román-Leshkov*

Effective hydrodeoxygenation of biomass-derived oxygenates is achieved with MoO_3 to produce unsaturated hydrocarbons, converting linear ketones and cyclic ethers to olefins, and cyclic ketones and phenolics to aromatics with high yields. The catalyst is selective for C–O bond cleavage and operates using low H_2 pressures (≤1 bar). We show that deactivation can be minimised by tuning hydrogen partial pressure, that original activity can be recovered by calcination, and that catalytic activity can be maintained in the presence of water. Theoretical calculations are used to elucidate reaction pathways and highlight the role of oxygen vacancies in the deoxygenation process.

Broader context

The transportation sector relies primarily on diminishing petroleum-based resources for fuel production. In recent years, the development of alternative methods to generate transportation fuels has been an important focus in the private and public sectors. Lignocellulosic biomass is an attractive source of renewable carbon for the production of fuels and chemicals. Of the many conversion processes, biomass fast pyrolysis has emerged as a viable technology for production of biomass-derived liquid fuels on a large scale. However, pyrolysis bio-oils are not fungible with current refinery streams, requiring upgrading steps to reduce acid, oxygen and water contents in the mixture. The key element to successfully upgrade bio-oils is the development of a catalytic system that can achieve deep deoxygenation, while minimizing hydrogen consumption and carbon loss. Catalysts must maintain high stability and recyclability in the presence of bulk water. In this contribution, we show that MoO_3 is an effective catalyst to transform several biomass-derived oxygenates into unsaturated hydrocarbons in high yields using low H_2 pressures. The catalyst is robust and its initial activity can be recovered by simple calcination. This material opens attractive avenues for the conversion of bio-oil components into hydrocarbons that can be easily blended with refinery streams.

Due to the ultimate depletion of petroleum and the rapidly increasing emissions of greenhouse gases, alternative energy sources must be developed to produce liquid fuels. Lignocellulosic biomass represents an attractive renewable feedstock that can help diversify transportation fuels, while reducing CO_2 emissions. Fast pyrolysis is an effective thermochemical route that transforms solid biomass into non-condensable gases, liquid bio-oil, and char. The bio-oil contains a wide range of oxygenated products that can be grouped into three main families of compounds: (1) small oxygenates (*e.g.*, acetic acid, glycolaldehyde, and acetol); (2) sugar-derived compounds (*e.g.*, furan derivatives and levoglucosan); and (3) lignin-derived compounds (*e.g.*, guaiacol, anisole, and phenol). Unfortunately, the direct utilisation of bio-oil as a transportation fuel is unfeasible due to its high acid, oxygen, and water contents. The widespread utilisation of bio-oil as a fuel precursor depends on the development of robust catalytic strategies to upgrade its components into fungible intermediates that can be integrated with current petroleum refinery streams.

Hydrodeoxygenation (HDO) is the most promising route to improve the effective H/C ratio of pyrolysis bio-oils and produce hydrocarbons either as final fuel components (*e.g.*, gasoline and diesel) or as fuel intermediates (small olefins and alkanes). The key challenge faced by HDO processes is achieving a high degree of oxygen removal, while minimising hydrogen consumption.[1] Several classes of catalysts can be used for HDO.[2] For example, precious metal catalysts (such as Pd, Pt, Rh, and Ru) and non-precious metal catalysts (such as Ni and Cu) are active for hydrogenation/hydrogenolysis reactions.[3] However, they require high H_2 pressures that inevitably saturate all double bonds, resulting, in some cases, in excessive H_2 consumption.[4] The industrial HDO catalysts based on Co–Mo–Ni formulations give a superior performance in HDO, but undergo rapid deactivation due to coke formation and water poisoning.[5]

The redox properties of certain metal oxides, such as molybdenum oxide (MoO_3), have been used to catalyse the oxidation of olefins to aldehydes and ketones.[6] It is proposed

Department of Chemical Engineering, Massachusetts Institute of Technology, Cambridge, MA, 02139, USA

† Electronic supplementary information (ESI) available. See DOI: 10.1039/c3ee24360e

that these catalysts operate by way of a Mars–van Krevelen mechanism wherein an oxygen atom located at the surface of the catalyst reacts with the olefinic compound to yield an oxygenated product plus an oxygen vacancy site (*i.e.*, an uncoordinated metal site on the metal oxide).[7] Recently, these catalysts have also been explored in HDO processes of small oxygenates under the premise that a reverse Mars–van Krevelen reaction would result in the removal of the oxygen atom from the oxy-compound upon the adsorption on the vacancy site with concomitant regeneration of the vacancy with H_2 to produce water (see Fig. 1).[8] This pathway is supported by the work of Moberg and co-workers, who demonstrated that the HDO of acrolein on MoO_3 to propylene is thermodynamically favourable at 593 K.[8b]

Here, we show that MoO_3 effectively catalyses the HDO of biomass-derived oxygenates using low H_2 pressures, converting linear ketones and cyclic ethers to olefins, and cyclic ketones and phenolics to aromatics with high selectivity. Experiments geared at evaluating the catalytic HDO performance were carried out in a low-pressure packed-bed reactor under conditions free of mass transfer limitations (see ESI†); and density functional theory (DFT) calculations aimed at understanding the role of oxygen vacancies in reactivity were performed on a small model cluster (Mo_3O_9) representative of the catalyst surface.[8b,9] Model compounds utilised in this study included acetone and 2-hexanone (derived from carboxylic acid condensation *via* ketonisation); cyclohexanone (derived from partial hydrogenation of phenolics); 2-methylfuran and 2,5-dimethylfuran (derived from partial deoxygenation of furfural and 5-hydroxymethylfurfural); and anisole (derived from lignin depolymerisation). The impact of H_2 and water partial pressures on catalyst performance was investigated given that both compounds directly influence oxygen vacancy generation on the catalyst surface.

An initial screening of reducible metal oxides indicated that MoO_3 is an attractive candidate for HDO. Using acetone as a model compound, HDO was investigated using various metal oxides, including V_2O_5, Fe_2O_3, CuO, WO_3, and MoO_3, that are active in oxidation reactions and that feature a wide range of M–O bond strengths.[10] All oxides were active HDO catalysts, with estimated specific acetone consumption rates of 14.2, 13.3, 10.9, 9.8 and 9.7 mmol m^{-2} h^{-1} for MoO_3, V_2O_5, Fe_2O_3, CuO and WO_3, respectively. Notably, MoO_3 featured the highest selectivity (98%) towards unsaturated hydrocarbons of all the metal oxides investigated (see Table S1†).

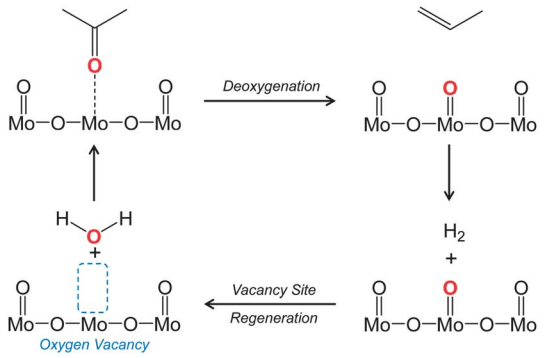

Fig. 1 Schematic representation of the molybdenum oxide redox cycle involved in the hydrodeoxygenation of acetone.

Table 1 shows the total conversion and the corresponding product distribution resulting from the reaction of model compounds with MoO_3 at 673 K and identical contact time (W/F, defined as g_{Cat} $(mmol_{Feed}\ h^{-1})^{-1}$). In all cases the HDO selectivity towards unsaturated hydrocarbons exceeded 97% regardless of the type of oxygenate used. For example, acetone was converted mainly into propylene, C_4–C_6 olefins, and alkylbenzenes with carbon yields of 67.2%, 28.1% and 1.6%, respectively. In a similar manner, hexenes and C_3–C_5 olefins were produced from 2-hexanone with 95% and 4% selectivity, respectively, at 81% conversion. In contrast to the conversion of acetone, no dimerised olefinic products were detected and rather hexadienes, the dehydrogenated products of hexenes, were observed in the conversion of 2-hexanone. The conversion of the cyclic ketone, cyclohexanone, followed a similar deoxygenation reaction pathway, generating first cyclohexene and subsequently benzene. These data show that the dehydrogenation of the deoxygenated product was more pronounced for a cyclic ketone (69% yield of benzene from cyclohexanone), than for an aliphatic ketone (6.2% yield of hexadienes from 2-hexanone). Interestingly, anisole was selectively converted to a mixture of aromatic products comprised of 38.7% benzene, 12.7% toluene, 4.2% xylenes, and 8.5% alkylbenzenes, suggesting that the catalyst promotes both deoxygenation and transalkylation reactions of this phenolic derivative. We note that no cyclohexane was observed during the conversion of anisole even at conversion levels below 10%, thus indicating that anisole deoxygenation following a pathway involving saturation of the ring followed by dehydration is unlikely and may instead undergo direct C–O bond cleavage (*vide infra*). Finally, the cyclic ethers, 2-methylfuran and 2,5-dimethylfuran, were converted to pentenes and hexenes, respectively. Overall mass balances generally exceeded 96%, with <1% of the carbon ending up as coke, as quantified from thermogravimetric analyses (TGA) of the spent catalysts.

An important feature of the MoO_3 catalyst is that the main reaction products contain the same number of carbon atoms as that of the parent reactant (*e.g.*, 2-hexanone is converted mainly into hexenes), thus indicating that C–O bonds are selectively cleaved without cleaving C–C bonds. Carbonyl-containing compounds are more reactive than ether-containing compounds. The specific rates obtained at low conversion for each compound (see Table S2†) show a reactivity trend of cyclohexanone > acetone > 2-hexanone > anisole ~ 2-methylfuran ~ 2,5-dimethylfuran. This trend correlates well with adsorption energies obtained from density functional theory (DFT) calculations that show the strongest heats of adsorption for the cyclic ketone (−188.6 kJ mol^{-1} for cyclohexanone), followed by linear ketones (−137.3 kJ mol^{-1} for 2-hexanone, and −131.2 kJ mol^{-1} for acetone), and finally by ether-containing compounds (−90.3 kJ mol^{-1} for anisole, −60.8 kJ mol^{-1} for 2,5-dimethylfuran, and −59.6 kJ mol^{-1} for 2-methylfuran). Adsorption structures and relevant bond distances are shown in Table S3.†

Table 1 Conversion and product distribution of oxygenated compounds on MoO_3 catalysts[a]

Feed	Ace	2-Hex	Cy-hex	Ani	MF	DMF
Conversion (C-mol%)	96.8	81.2	100.0	65.0	53.1	43.4
Selectivity to HCs	99.7	99.4	99.7	98.6	97.4	98.8
Yield (C-mol%)						
Hydrocarbons						
Propylene	67.2	1.1	0	0	4.3	2.8
Butenes	7.9	1.0	0	0	1.3	1.7
Pentenes	2.4	0.6	0	0	43.5	0.3
Pentadienes	0	0.3	0	0	2.6	0.3
Methylpentadienes	0	0	2.7	0	0	0
Hexenes	14.0	71.5	0	0	0	28.8
Hexadienes	3.8	6.2	0	0	0	9.1
Cyclohexene	0	0	20.9	0	0	0
Benzene	0	0	69.0	38.7	0	0
Toluene	0	0	0	12.7	0	0
Xylenes	0	0	0	4.2	0	0
Alkylbenzenes	1.6	0	0	8.5	0	0
Biphenyl	0	0	7.1	0	0	0
Oxygenates						
Pentanone	0	0	0	0	0.8	0
Hexanone	0.3	0	0	0	0	0
Coke	0.4	0.5	0.3	0.9	0.6	0.5
Specific rate[b] (mmol h^{-1} g_{Cat}^{-1})	67.8	51.9	115.8	24.7	20.3	19.1

[a] Feed legend: acetone (Ace), 2-hexanone (2-Hex), cyclohexanone (Cy-hex), anisole (Ani), 2-methylfuran (MF), and 2,5-dimethylfuran (DMF). *Reaction conditions*: $T = 673$ K, $P_{Total} = 1.013$ bar (0.032 bar P_{Feed}, 0.196 bar P_{H_2}; balance He), $W/F = 0.068$ g_{Cat} $(mmol_{Feed}\ h^{-1})^{-1}$, and TOS = 1 h. Conversion % = (carbon moles of reactant consumed/carbon moles of reactant input) × 100%. Selectivity to olefins% = (carbon moles of total olefin product/carbon moles of reactant consumed) × 100%. Yields% = (carbon moles of product/carbon moles of reactant input) × 100%. Coke yield on spent catalysts was calculated from the weight loss determined by TGA. [b] The specific rate was calculated based on carbon moles of reactant consumed per catalyst weight per unit time at conversions <20% (see Table S2†).

Our experimental data indicate that the presence of H_2 plays a crucial role in the HDO activity on the MoO_3 catalyst. As shown in Fig. 2, replacing H_2 with an inert gas during the course of the reaction resulted in a drastic decrease in conversion of acetone, 2-hexanone, and anisole feeds. Resuming H_2 flow restored the catalytic activity and, although overall conversion diminished, the product selectivity remained constant before and after reinitiating the H_2 flow. The effect of H_2 was investigated further by conducting a series of experiments at varying H_2 partial pressures (*i.e.*, changing H_2 content in the sweep gas from 10% to 100% at a constant carrier flow of 70 ml min^{-1}) during the conversion of 2-hexanone (see Fig. 3). The experiments were carried out over the same catalyst bed which was regenerated after each run by *in situ* calcination under air flow at 873 K for 1 h. Note that the catalyst can be regenerated back to its original activity by this calcination procedure. As expected, H_2 partial pressure had a strong effect on catalyst performance, with 2-hexanone conversion increasing from 60% to 99% when the H_2 content in the sweep gas was increased from 10% to 100%. Moreover, the partial pressure of H_2 also affected the

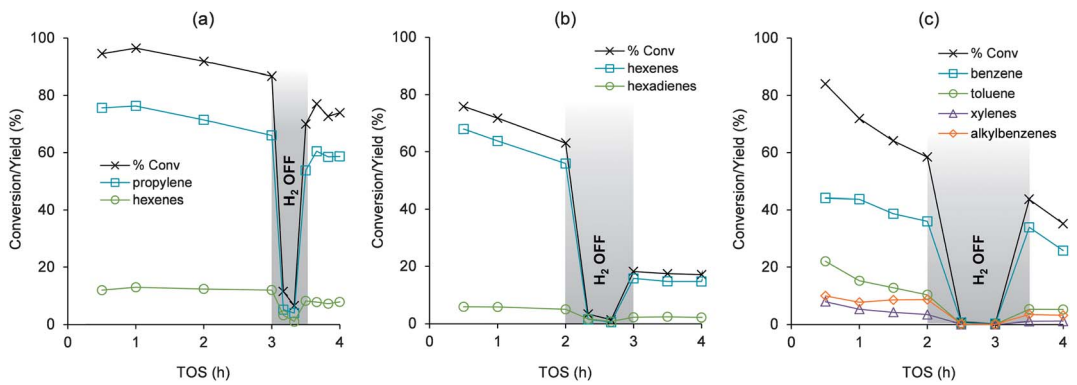

Fig. 2 Conversion and product distribution as a function of time-on-stream (TOS) using (a) acetone, (b) 2-hexanone, and (c) anisole feeds. *Reaction conditions*: $T = 673$ K; $P_{Total} = 1.013$ bar (0.032 bar P_{Feed}, 0.196 bar P_{H_2}, balance He); $W/F = 0.068$ g (mmol h^{-1})$^{-1}$ for acetone, 0.059 g (mmol h^{-1})$^{-1}$ for 2-hexanone, and 0.075 g (mmol h^{-1})$^{-1}$ for anisole. Minor products (yields < 5%) are not shown.

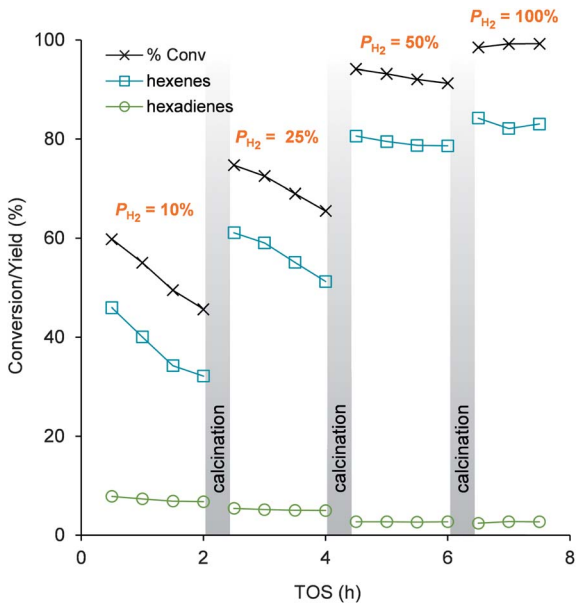

Fig. 3 Effect of H_2 partial pressure on 2-hexanone conversion. *Reaction conditions*: $T = 673$ K, $P_{Total} = 1.013$ bar (0.032 bar $P_{2\text{-Hexanone}}$; 0.098, 0.245, 0.491, and 0.981 bar P_{H_2} corresponding to 10%, 25%, 50%, and 100% H_2 concentration in the carrier gas, respectively; balance He), and $W/F = 0.056$ g (mmol $h^{-1})^{-1}$. Minor products (yields < 5%) are not shown in the figure.

catalyst's deactivation profile. Specifically, the slope of the deactivation profile became less negative (*i.e.*, approached zero) as H_2 partial pressure was increased, suggesting that H_2 is critically involved in regenerating active oxygen vacancy sites and in preventing site blocking by carbonaceous species. These data are consistent with the dependency of oxygen vacancy concentration on hydrogen and water pressure derived by Moberg and co-workers.[8b]

In contrast to 2-hexanone, H_2 pressure has a strong influence on the product distribution of acetone HDO. As seen from Fig. S1,† upon increasing H_2 pressure from 0.193 bar to 0.965 bar, not only did the overall conversion increase from 61% to 96% but also propylene selectivity increased from 44% to 65%. Lower propylene selectivity is observed due to competing parallel reactions (*e.g.*, condensation of acetone to hexanone) which yield higher molecular weight hydrocarbons.

Varying contact time also changes product distribution (see Fig. S2†). Specifically, for acetone HDO, a low W/F (0.0032 g_{Cat} (mmol $h^{-1})^{-1}$) shows the presence of two parallel reaction pathways: (1) HDO of acetone to propylene (44% selectivity); and (2) condensation of acetone to hexanone (32% selectivity), which consecutively undergoes HDO to hexenes (14% selectivity). At a higher W/F, the decrease in hexanone selectivity is observed with a corresponding increase in propylene and hexene selectivity. A decrease in H_2 partial pressure results in decreased HDO activity, which can be compensated by increasing the W/F. For instance, for a reaction with a W/F of 0.037 g_{Cat} (mmol $h^{-1})^{-1}$, the HDO selectivity decreases from 99.9% (at 97.1% conversion) to 93.4% (at 60.7% conversion) when H_2 pressure is decreased from 0.973 to 0.193 bar. However, increasing the W/F to 0.068 g_{Cat} (mmol $h^{-1})^{-1}$ at 0.193 bar H_2 generates a 99.7% olefin selectivity at 96.8% conversion (see Fig. S2b†).

HDO reactions of aqueous acetone solutions were performed to study the impact of water on catalyst activity. Fig. 4 shows the comparison of acetone conversion under different reaction conditions in which the partial pressure of acetone was kept constant, while the concentrations of water and hydrogen were adjusted. The conversion of acetone decreased from 96% to 73% when the feed was changed from pure acetone (0.048 bar $P_{Acetone}$, 0.965 bar P_{H_2}) to a 6 : 4 w/w acetone : water mixture (0.048 bar $P_{Acetone}$, 0.104 bar P_{H_2O}, 0.861 bar P_{H_2}). The decrease in catalytic activity was more pronounced at lower H_2 partial pressures. For instance, for the 6 : 4 w/w acetone : water mixture feed, the conversions of acetone were reduced by 22.7%, 27.1% and 29.7% when using H_2 partial pressures of 0.861, 0.431, and 0.172 bar, respectively (see Table S4†). Therefore, the water site-blocking effect can be minimised by increasing the H_2 concentration. Similar conversions were obtained from the pure acetone feed (10 : 0 w/w acetone : water mixture) ran with $P_{H_2} = 0.482$ bar, as with a 6 : 4 w/w acetone : water mixture feed ran with $P_{H_2} = 0.861$ bar. Notably, even in the presence of large amounts of water, the selectivity towards unsaturated hydrocarbon products (mainly propylene and hexenes) always exceeded 90% at high conversions. While the addition of water negatively impacted the overall HDO activity, it did not accelerate catalyst deactivation. As shown in Fig. S3,† the deactivation rate derived from the reaction of an 8 : 2 w/w acetone : water mixture feed was comparable to that of a pure acetone feed, but took place at a lower conversion level (*vide infra*).

Due to the presence of parallel side reactions, temperature alters acetone's HDO product distribution. Table S5† shows conversion and product yields obtained in the temperature

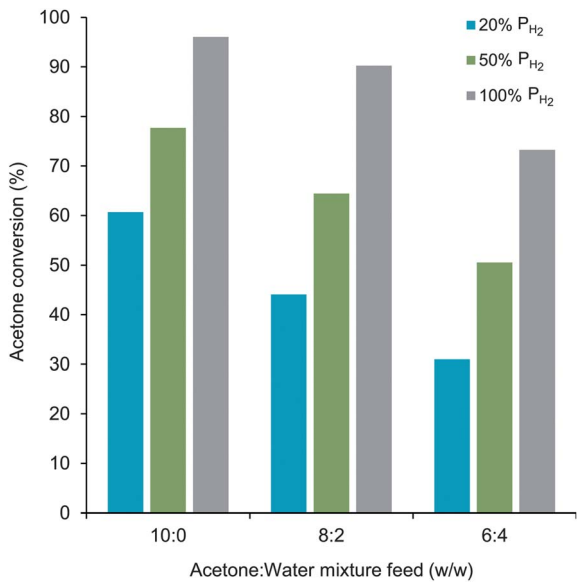

Fig. 4 Effect of water content and H_2 partial pressure on acetone conversion. *Reaction conditions*: $T = 673$ K, $P_{Total} = 1.013$ bar (0.048 bar $P_{Acetone}$, see P_{H_2O} and P_{H_2} of each run in Table S4†), $W/F = 0.037$ g (mmol $h^{-1})^{-1}$, and TOS = 1 h.

range from 523 to 673 K. At 523 K and a corresponding conversion of 14%, the selectivity values to hexanone and to olefins are 32% and 68%, respectively. At 573 K, the olefin selectivity increased to 83.2% at 45% conversion. Propylene selectivity was ~40% both at 523 and 573 K thus suggesting that increased olefin selectivity is obtained from the conversion of hexanone to hexenes. Olefin selectivity improved further at higher temperatures, reaching 98% at 74% conversion at 673 K. Importantly, propylene selectivity increased to 61%, indicating that the HDO rate is greater than the condensation rate either due to an increased concentration of vacancy sites or a larger HDO activation energy when compared to the condensation pathway.

Catalyst deactivation was profiled over a period of 24 h for various contact times (see Fig. S3a†). A first order decay kinetic model was used to describe the decrease in activity of acetone HDO over the MoO_3 catalyst. As shown in Fig. S3b, evaluation of the fractional conversion at constant W/F as a function of time-on-stream suggests the existence of two distinct deactivation modes. Importantly, the original activity can be recovered after a calcination process at 873 K for 1 h.

Combined characterization techniques and theoretical calculations were used to elucidate the impact of water on oxygen vacancy concentration. Analyses of catalysts after reaction indicate that the solid remains in the MoO_3 phase under the operating conditions (*i.e.*, $T = 623$ K, H_2 partial pressure ≤ 1 bar). The powder X-ray diffraction (PXRD) patterns of both freshly calcined and reduced samples showed identical peaks, suggesting the presence of a pure MoO_3 phase (see Fig. S4†). The X-ray photoelectron spectrum (XPS) of these two samples exhibited the same characteristic doublet Mo 3d peaks found in hexavalent molybdenum at ~235.9 and ~232.8 eV, which correspond to Mo $3d_{3/2}$ and Mo $3d_{5/2}$ orbitals, respectively (see Fig. S5†).[11] A temperature programed reduction (TPR) analysis suggests that the reduction of MoO_3 to MoO_2 is less likely to occur at temperatures below 873–1073 K.[12] Even though the partial surface reduction of MoO_3 to form oxygen vacancies was undetectable by PXRD and XPS techniques, their formation is thermodynamically favourable. DFT calculations show a Gibbs free energy of oxygen vacancy generation of 60.6 kJ mol^{-1} at 673 K, which translates to ~5% of surface oxygen that can be removed to generate vacancies sites. Table S6† shows the corresponding concentration of oxygen vacancy sites with varying H_2 and water partial pressures. It is observed that regardless of the operating H_2 pressures, changing acetone : water mixture feeds from 8 : 2 to 6 : 4 w/w results in a decrease of the surface oxygen vacancy density by ~30%.

Several possible reaction mechanisms have been proposed for HDO reactions of oxygenates using reducible metal oxides.[2] For MoO_3 catalysts, it has been shown that surface oxygen vacancies play a central role in the HDO process.[8b,c] In this regard, we hypothesise that oxygenated compounds interact with oxygen vacancies to form the Mo–O bond, followed by cleavage of the C–O bond, and desorption of the resulting hydrocarbon products. Accordingly, the conversion of oxygenates into unsaturated hydrocarbons requires the concerted action of two cycles: one wherein H_2 reduces the oxidised catalyst surface and a second wherein the reduced catalyst surface is oxidised by the oxygenated molecule. We performed density functional calculations to elucidate the energetics involved in both processes.

We investigated the oxygen vacancy site creation process, including the adsorption of hydrogen, the formation of surface hydroxyl groups, and the desorption of water to generate an active vacancy site, using a Mo_3O_9 cluster as a model of the fully oxidised MoO_3 surface. The first step in this process is the adsorption of hydrogen, which can occur at different locations of surface oxygens, namely, terminal and bridging sites (see Table S7†). The adsorption on two terminal oxygen sites has the highest stability (−37.5 kJ mol^{-1}), followed by the adsorption on one terminal and one bridging site with lower stability (−3.8 kJ mol^{-1}). The adsorption solely on bridging sites was highly unfavourable (+53.2 kJ mol^{-1}). In this regard, the absorption of hydrogen on a bridging site is less stable than that on a terminal site or, in other words, this hydrogen is more reactive and behaves as a strong Brønsted acid. Next, we investigated the formation of water *via* the transfer of a hydrogen atom to a terminal hydroxyl oxygen. As depicted in Fig. 5, the first pathway starts from the most stable intermediate, **2a**, which contains two terminal hydroxyl groups. A proton is transferred to another hydroxyl group *via* transition state **3a** to form the absorbed water, **4**. This step requires an activation barrier of 98.9 kJ mol^{-1}. Proton nuclear magnetic resonance (^{1}H NMR) studies have shown that hydrogen mobility on molybdenum oxides is relatively facile and requires an activation energy for diffusion around 10–30 kJ mol^{-1}, depending on the H_2 concentration.[13] This implies that the migration of a proton from a terminal oxygen site to a bridging site, and *vice versa*, is favourable. Therefore, another route for oxygen vacancy creation could have started from **2b**, which contains one bridging and one terminal hydroxyl group, even though it shows a lower stability than that of **2a**. Interestingly, the corresponding activation energy found for the formation of transition state **3b** was substantially lower (32.5 kJ mol^{-1}), suggesting a more kinetically favourable reaction pathway. This observation can be explained by a shorter proton migration from the bridging to the terminal sites. The final step, **5**, is the desorption of water and the formation of oxygen vacancy sites. The overall oxygen vacancy creation process is endothermic, demanding 90.3 kJ mol^{-1}, which is in agreement with previous results obtained from a slab model.[14]

Next, to gain a better understanding of the HDO process, the Mo–O bond forming and the C–O bond breaking events occurring in the catalytic cycles were analysed based on the relevant bond energies (see Table S8†). The average bond dissociation energies follow an order of R=O > Mo=O > Ar–OH > Ar–OR > R–OH > R–OR. The C=O bond of the carbonyl-containing molecules, such as acetone, 2-hexanone and cyclohexanone, shows the highest bond energy, and exceeds the energy of a surface Mo=O bond. Therefore, a route involving direct C=O bond cleavage is thermodynamically unfavourable since the energy gained from the Mo=O bond formation is less than the energy required for breaking the C=O bond. From the experimental results, it is observed that a carbonyl compound readily undergoes HDO under the reaction conditions

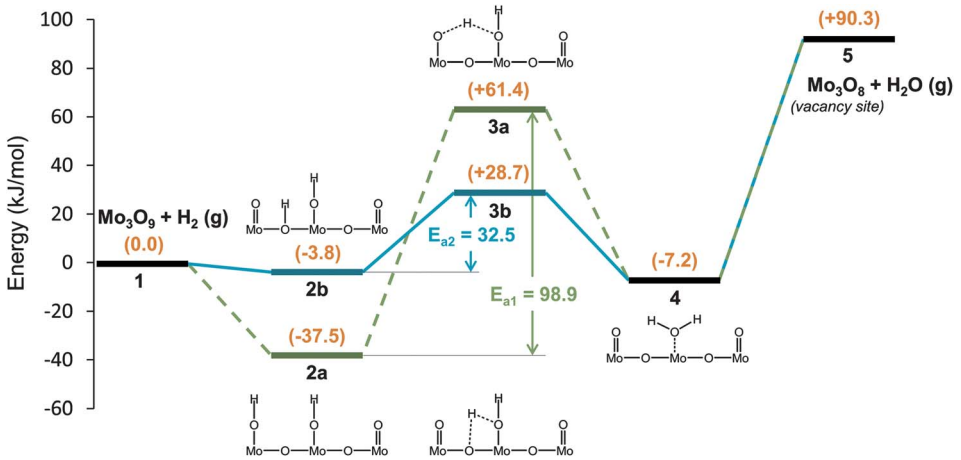

Fig. 5 Energy profiles for oxygen vacancy site generation on a simulated molybdenum oxide surface.

examined, suggesting that hydrogen transfer is an important step for converting the C(sp^2)–O to a weaker C(sp^3)–O, which allows easier C–O bond breaking. A recent DFT study showed that the hydrogenation of acrolein into allyl alcohol is energetically feasible over MoO_3.[8b] However, in the present study, no alcohol products were detected even at conversions <7% (see Table S2†). It is plausible that only one hydrogen is transferred to the carbonyl carbon, resulting in the C–O bond weakening and breaking, rather than the saturation of C=O to alcohols; or that the intermediate alcohol species is immediately dehydrated at the reaction temperature (*i.e.*, 673 K). Further spectroscopic and theoretical investigations are needed to rule out either of these options. Unlike ketones, ether-containing molecules, such as anisole, 2-methylfuran and 2,5-dimethylfuran, already possess a weaker C–O bond than the Mo–O bond; thus the C–O bond breaking and the Mo–O bond forming will lead to a positive net energy gain, suggesting that the HDO process is energetically favourable. In the case of anisole, there is a debate on reaction pathways associated with the elimination of oxygen from the molecule. From the analysis of bond dissociation energies (see Table S8†), the Ar–OR bond (*i.e.*, anisole, 422 kJ mol^{-1}) and the Ar–OH bond (*i.e.*, phenol, 468 kJ mol^{-1}) are weaker than the surface Mo–O bond (575 kJ mol^{-1}). Therefore, over the MoO_3 catalyst, it is thermodynamically conceivable that direct C–O cleavage may occur (*e.g.*, as it would occur in a reverse MvK mechanism) preferentially over the partial aromatic hydrogenation followed by a dehydration route. This is consistent with our experimental data showing no evidence of ring saturation even at low conversion for the anisole or cyclohexanone feeds. In contrast to the HDO on MoO_3, a bifunctional metal–acid catalyst requires aromatic ring hydrogenation to achieve a weaker R–OR bond for anisole (339 kJ mol^{-1}) and R–OH bond for the phenol (385 kJ mol^{-1}) bond. Such bond weakening would allow the dehydration of the ether/alcohol species to occur. Considering the number of C–O bonds appearing in the molecules, the removal of oxygen from ethers requires two C–O bond breaking, while only one C–O bond needs to be cleaved in the case of ketones. As a result, the HDO activities for the ether compounds are prone to be lower than that for the ketones as observed in our experimental results (see Table 1). Note that for all compounds, the C–O bonds can be further weakened upon the adsorption at the oxygen vacancy sites, as estimated by the elongation of the C–O bonds (see Table S3†).

Conclusion

We have shown that MoO_3 is a promising catalyst for the HDO of biomass-derived oxygenates into unsaturated hydrocarbons. The catalyst is capable of processing various oxygenate feeds with high activity and selectivity using low H_2 pressures. MoO_3 exhibits high tolerance to coke formation and water poisoning. Importantly, in the case of deactivation, it can be regenerated by calcination without losing its initial activity. Although the HDO products (*i.e.*, small olefins and aromatics) are not ready to be directly used as conventional gasoline (C_5–C_{12}) and diesel (C_{13}–C_{22}) fuels, they can be upgraded with well-established methods, such as oligomerisation, alkylation, reforming and isomerisation, intended to extend and/or branch the carbon backbone.

Further studies are needed to characterise the dynamics of surface oxygen vacancy generation and to convert other molecules featuring functional groups commonly found in bio-oil oxygenates (*e.g.*, acetic acid and glycolaldehyde).[15] To this end, our preliminary results show that the MoO_3 catalyst is active in deoxygenating aqueous solutions of acetic acid (1 : 1 w/w). Detectable products include CO_2, ethane/ethylene, propylene, acetaldehyde and acetone, suggesting the presence of several parallel reaction pathways including: (1) ketonisation of acetic acid to acetone, water, and CO_2; (2) partial HDO of acetic acid to acetaldehyde, and (3) HDO of acetaldehyde and acetone to ethane/ethylene and propylene, respectively. Understanding the HDO of organic acids is one of our current objectives.

Acknowledgements

This research was funded by British Petroleum (BP) through the MIT Energy Initiative Advanced Conversion Research Program.

Generous allocations of computing time were provided by the OU Supercomputing Center for Education and Research (OSCER) at the University of Oklahoma. The authors would like to thank Yuran Wang for the XPS analysis of the catalyst samples.

References

1 D. E. Resasco, *J. Phys. Chem. Lett.*, 2011, **2**, 2294–2295.
2 Z. He and X. Wang, *Catal. Sustainable Energy Prod.*, 2012, **1**, 28–52.
3 (*a*) R. C. Runnebaum, T. Nimmanwudipong, D. E. Block and B. C. Gates, *Catal. Sci. Technol.*, 2012, **2**, 113–118; (*b*) S. Sitthisa and D. E. Resasco, *Catal. Lett.*, 2011, **141**, 784–791; (*c*) S. Sitthisa, T. Pham, T. Prasomsri, T. Sooknoi, R. G. Mallinson and D. E. Resasco, *J. Catal.*, 2011, **280**, 17–27.
4 (*a*) C. R. Lee, J. S. Yoon, Y.-W. Suh, J.-W. Choi, J.-M. Ha, D. J. Suh and Y.-K. Park, *Catal. Commun.*, 2012, **17**, 54–58; (*b*) M. V. Bykova, D. Y. Ermakov, V. V. Kaichev, O. A. Bulavchenko, A. A. Saraev, M. Y. Lebedev and V. A. Yafkovlev, *Appl. Catal., B*, 2012, **113–114**, 296–307.
5 (*a*) M. Badawi, J. F. Paul, S. Cristol, E. Payen, Y. Romero, F. Richard, S. Brunet, D. Lambert, X. Portier, A. Popov, E. Kondratieva, J. M. Goupil, J. El Fallah, J. P. Gilson, L. Mariey, A. Travert and F. Maugé, *J. Catal.*, 2011, **282**, 155–164; (*b*) E. Laurent and B. Delmon, *J. Catal.*, 1994, **146**, 281–291; (*c*) O. İ. Şenol, T.-R. Viljava and A. O. I. Krause, *Catal. Today*, 2005, **106**, 186–189.
6 (*a*) S. Tan, Y. Moro-Oka and A. Ozaki, *J. Catal.*, 1970, **17**, 132–142; (*b*) S. A. Stevenson and W. Liang, Preparation of mixed metal oxide catalysts for catalytic oxidation of olefins to unsaturated aldehydes, *US Pat.*, 6 946 422, 20 September 2005.
7 (*a*) R. K. Grasselli, *Top. Catal.*, 2002, **21**, 79–88; (*b*) P. Mars and D. W. van Krevelen, *Chem. Eng. Sci.*, 1954, **3**, 41–59; (*c*) R. K. Grasselli and J. D. Burrington, *Adv. Catal.*, 1981, **30**, 133–163; (*d*) S. Pudar, J. Oxgaard, K. Chenoweth, A. C. T. van Duin and W. A. Goddard III, *J. Phys. Chem. C*, 2007, **111**, 16405–16415.
8 (*a*) D. Mei, A. M. Karim and Y. Wang, *J. Phys. Chem. C*, 2011, **115**, 8155–8164; (*b*) D. R. Moberg, T. J. Thibodeau, F. G. Amar and B. G. Frederick, *J. Phys. Chem. C*, 2010, **114**, 13782–13795; (*c*) T. J. Thibodeau, A. S. Canney, W. J. DeSisto, M. C. Wheeler, F. G. Amar and B. G. Frederick, *Appl. Catal., A*, 2010, **388**, 86–95; (*d*) T. Matsuda, Y. Hirata, H. Sakagami and N. Takahashi, *Chem. Lett.*, 1997, **12**, 1261–1262; (*e*) T. Matsuda, Y. Hirata, S. Suga, H. Sakagami and N. Takahashi, *Appl. Catal., A*, 2000, **193**, 185–193.
9 (*a*) S. Pudar, J. Oxgaard, K. Chenoweth, A. C. T. van Duin and W. A. Goddard III, *J. Phys. Chem. C*, 2007, **111**, 16405–16415; (*b*) R. Tokarz-Sobieraj, M. Witko and R. Grybos, *Catal. Today*, 2005, **99**, 241–253; (*c*) J. Wang, Y. Su, J. Xu, C. Ye and F. Deng, *Phys. Chem. Chem. Phys.*, 2006, **8**, 2378–2384; (*d*) D. Zeng, H. Fang, A. Zheng, J. Xu, L. Chen, J. Yang, J. Wang, C. Ye and F. Deng, *J. Mol. Catal. A: Chem.*, 2007, **270**, 257–263.
10 (*a*) K. Alexopoulos, M.-F. Reyniers and G. B. Marin, *J. Catal.*, 2012, **295**, 195–206; (*b*) Y. Sakata, C. A. van Tol-Koutstaal and V. Ponecz, *J. Catal.*, 1997, **169**, 13–21.
11 C. D. Wagner, W. M. Riggs, L. E. Davis and J. F. Moulder, in *Handbook of X-ray Photoelectron Spectroscopy*, ed. G. E. Muilenberg, Minnesota, USA, 1979.
12 S. Majumdar, I. G. Sharma, I. Samajdar and P. Bhargava, *Metall. Mater. Trans. B*, 2008, **39**, 431–438.
13 C. Ritter, W. Müller-Warmuth and R. J. Schöllhorn, *Chem. Phys.*, 1985, **83**, 6130–6138.
14 R. Tokarz-Sobieraj, M. Witko and R. Grybos, *Catal. Today*, 2005, **99**, 241–253.
15 (*a*) M. Łabanowska, *Phys. Chem. Chem. Phys.*, 1999, **1**, 5385–5392; (*b*) M. Dieterle, G. Weinberg and G. Mestl, *Phys. Chem. Chem. Phys.*, 2002, **4**, 812–821.

